Heliyon 10 (2024) e25712

Contents lists available at ScienceDirect

Heliyon

journal homepage: www.cell.com/heliyon

Research article

Dual-band independently tunable 8-element MIMO antenna for 5G smartphones

Ali Sufyan [a,*], Khan Bahadar Khan [a], Xingliang Zhang [b], Tauseef Ahmad Siddiqui [a], Abdul Aziz [a]

[a] Faculty of Engineering, The Islamia University of Bahawalpur, Bahawalpur, Punjab 63100, Pakistan
[b] School of Information and Communication Engineering, Dalian University of Technology, Dalian, Liaoning, China

A B S T R A C T

In this paper, a multi-input multi-output (MIMO) antenna for future mobile phone applications operating in sub-6 GHza using a novel combination of an E-shaped slot placed on the ground plane and an F-shaped probe is used to achieve a dual-band independently tunable antenna. The proposed antenna is not only self-isolated but it has also effectively achieved high isolation of greater than 17 dB in both 3.5 GHz (3.4 – 3.6 GHz) and 4.7 GHz (4.6 – 4.87 GHz) frequency bands for 8-element MIMO antenna configuration for 5G smartphones. The simple yet compact size of (0.035 λ_0 × 0.23 λ_0), of the slot antenna produces a balanced slot mode which not only reduces the ground effects but also improves the isolation between two adjacent input ports. The novelty of the proposed dual-band MIMO antenna is its independent control of each band across a wide frequency band and results demonstrate higher efficiency (64% – 71%) and diversity gain performance in both frequency bands. Furthermore, the antenna is designed by the meticulous configurations of 8-antenna elements without employing any external decoupling structure to attain the desired polarization diversity. The prototype of this 8-element MIMO antenna is also fabricated and measured to validate its simulated performance. The simple structure of the proposed design and high efficiency makes it a promising candidate for 5G smartphones.

1. Introduction

Fifth generation (5G) networks have become the major development trend to achieve the required spectral efficiency, bandwidth, and channel capacity. The C-band (3300-4200 and 4400-5000 MHz) is evolving as a principal frequency band for the development of 5G by offering an ideal harmony among coverage and capacity with respect to cost-effective implementation and is considered the primary band of interest across the world for 5G communication. Massive-MIMO frameworks with various antennas can attain high data rates and it is consequently one of the focus advancements in 5G systems [1]. However, the limited space in smartphones is a major challenge for the designers to load several antennas, which is the primary reason for reduced isolation and lower spectral efficiency. A MIMO antenna with higher isolation between antenna elements and wide bandwidth or multiband operation is highly preferred due to its increased spectral efficiency. However, a multiband antenna with independent tuning in each frequency band to achieve higher spectral efficiency for 5G smartphones is a challenging task. Several MIMO antennas are proposed in the literature for 5G smartphones having high isolation [2,3], low profile [4], and multiband operation using monopoles [5], dipoles [6], [7], and patch antennas [8,9]. However, design complexity [10], lower radiation efficiency [10,11], and higher ECC [8,10] are major drawbacks of such designs. A 10 × 10 dual-band MIMO antenna is presented in [12], which employs a neutralization line decoupling structure. However, it achieves only 12 dB isolation and 45% efficiency.

* Corresponding author.
E-mail address: ali.sufyan@iub.edu.pk (A. Sufyan).

https://doi.org/10.1016/j.heliyon.2024.e25712
Received 9 March 2023; Received in revised form 5 December 2023; Accepted 1 February 2024

Available online 9 February 2024

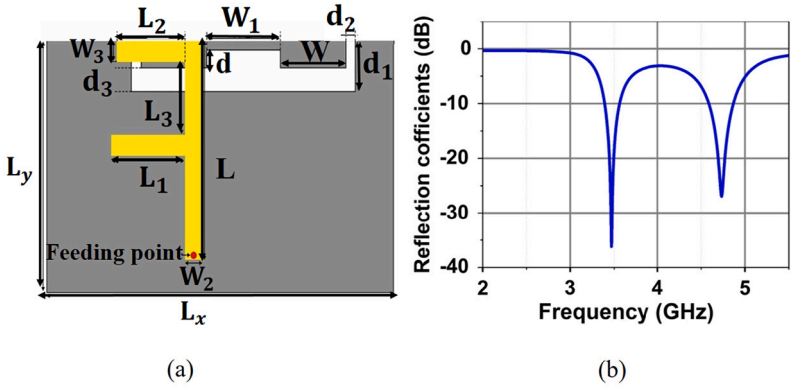

Fig. 1. (a) Detailed geometry and dimensions of the proposed dual-band antenna element, (b) reflection coefficient.

A dual-band low profile frequency reconfigurable MIMO antenna that is capable of concurrent tuning of both frequency bands and independent control of antenna over a broad frequency covering from 1.7 GHz to 3.8 GHz, is presented in [13] by using varactor diode. However, the varactor diode may increase fabrication complexity and greatly affects the antenna performance because of its nonlinear behavior. Similarly in [14], a wide-band antenna is investigated for 5G operating in the sub-6 GHz frequency spectrum by a hexagonal split-ring resonator covering 2.85 to 5.35 GHz (50%) bandwidth. Although the antenna has good impedance bandwidth, however, its radiation performance is not impressive due to the intrinsic loss of the metals used and the structural limitations of the split-ring resonator. A slot antenna has numerous advantages, such as planar profile, lightweight, two-fold polarization, multi-band and wideband characteristics, and easy integration with circuit elements [15,16]. However, there is still need to achieve a multiband-band independently tunable MIMO antenna with high radiation efficiency and isolation, particularly for 5G smartphones operating in C-band.

In this paper, a novel dual-band-independently tunable 8-element MIMO slot antenna is proposed for 3.5 GHz (3.4-3.6 GHz) and 4.7 GHz (4.6-4.87 GHz) frequency bands for 5G smartphones. It achieves higher isolation of greater than 17 dB. The major characteristics of the proposed MIMO antenna are summarized as follows:

- A novel dual-band-independent control antenna using a unique combination of an F-shaped probe and an E-shaped slot.
- The design is simple using slots, compact, and proposed without using any external decoupling structure.
- The antenna element is effectively covering the sub-6 GHz frequency spectrum to achieve the required spectral efficiency.
- The eight antenna elements are precisely arranged on the smartphone chassis with two of them are arranged orthogonally to accomplish high polarization diversity.

The parametric study is executed to calculate several parameters as the function of independent frequency control. Furthermore, to validate the design concept, the proposed 8-element MIMO antenna array is also fabricated and verified. The experimental outcome shows that the proposed design is effectively capable to attain high isolation (>17 dB), realized peak gain of 2.8 dBi and 3.2 dBi for the lower and upper band, respectively, with peak efficiencies of 64 & 71%, respectively. Finally, the MIMO antenna performance is also verified through envelope correlation coefficient (ECC), and diversity gain (DG). The rest of the article is arranged as follows. In Section 2, the design process is given together with the antenna geometry details. In Section 3, the experimental results are comprehensively compared with the simulated results, and the radiation patterns of the dual-band antenna are also analyzed. Lastly, the article is concluded in Section 4.

2. Design of dual-band antenna element

This section describes the basic design process of a dual-band slot antenna and the evolution of the designed antenna geometry.

2.1. Antenna configuration

The comprehensive structure of the proposed independently tunable dual-band E-shaped slot antenna element etched over the system ground plane is presented in Fig. 1(a). The antenna is fed via an F-shaped feeding strip on the other side of the substrate, which can excite the dual independently controlled resonant modes. The proposed slot antenna element is compatible with smartphone handsets due to its compact size (3 mm × 20 mm, that is 0.035 λ_0 × 0.23 λ_0). The FR4 dielectric material (loss tangent = 0.02 and, relative permittivity = 4.4) is used as a substrate for the proposed design. The optimal parameters of the antenna geometry are tabulated in Table 1. The reflection coefficient for the dual-band antenna is presented in Fig. 1 (b). It can be noticed that the dual-band antenna effectively operates at 3.5 GHz (3.4-3.6 GHz) and 4.7 GHz (4.6 - 4.87 GHz) frequency bands. The impedance bandwidths for both frequency bands are wide enough to meet the operational sub-6 GHz frequency bandwidth requirement for 4G/5G smartphones and to achieve high spectral efficiency.

Table 1
Optimal parameters of the antenna.

Parameter	L	L_1	L_2	L_3	W	W_1	W_2	W_3	d	d_1	d_2	d_3	L_x	L_y
Value (mm):	16.5	5.5	5.2	5.3	5.7	6.6	1.5	1.5	1.5	2.5	0.5	1	38	20

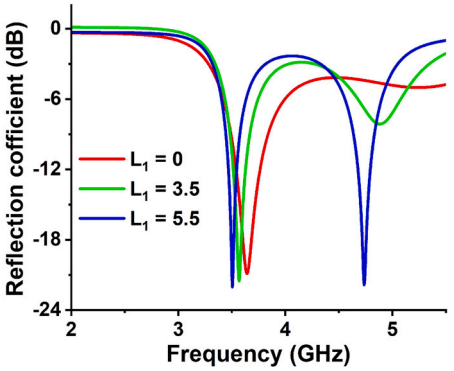

Fig. 2. Evolution of the proposed dual-band antenna due to variation in length L1 of the additional stub.

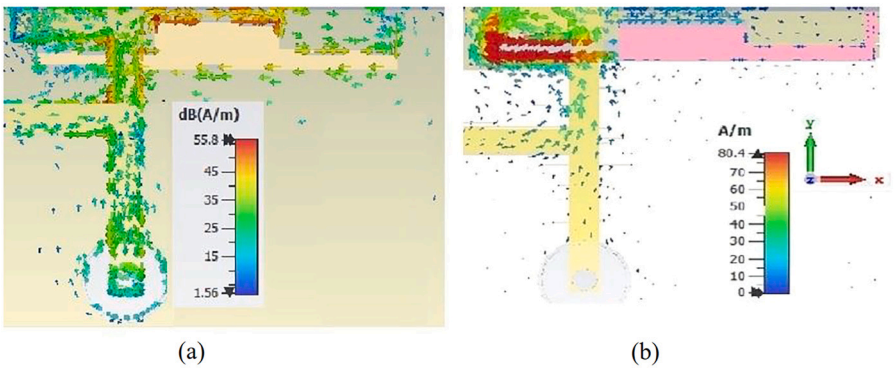

Fig. 3. Surface current distribution (a) 3.5 GHz band, (b) 4.7 GHz band.

2.2. Evolution of the dual-band element

The proposed dual-band element is evolved through the transformation of a single-band element proposed in [2], in which an L-shaped probe is used to excite the single resonant mode. In our proposed design the L-shaped probe is transformed perceptively to an F-shape by another additional horizontal stub to the L-shaped probe, which helps to excite another independent resonant mode in the E-shaped slot antenna. The reason for the additional resonance mode in the E-shaped slot antenna is explained well through the parametric analysis for the length L_1 of the additional stub, in Fig. 2.

It can be observed that the proposed element has a single resonant frequency at about 3.5 GHz for $L_1 = 0$, if we increase the length L_1 of the additional stub then a second resonant mode also appears at about 4.7 GHz. The surface current distributions for the dual-band antenna element at both frequency bands are also analyzed to explain the reason for the dual resonant modes and depicted in Fig. 3 (a) and (b), respectively. It can be seen that there is a strong focus of current distribution only on the middle edge of the E-shaped slot at 3.5 GHz, while at 4.7 GHz, the surface current distribution is focused on the left edge of the E-shaped slot. As the surface current distributions at both frequencies are focused on two different parts of the E-shaped slot, so resonant frequency of these modes can be controlled independently. Moreover, it can also be seen that the surface current distribution at both frequencies remained focused within the E-shaped slot and not extended towards the outside of the slot, which may help to achieve a higher level of isolation at both frequencies in the MIMO antenna configuration.

2.3. Independent control for dual-resonant modes

To demonstrate independent control of the two resonant frequencies, the parametric analysis is shown in Fig. 4 for the parameters that can control both resonant modes independently. As the maximum current is focused on the center edge of the E-shaped slot at 3.5 GHz, so, the lower resonant frequency can be easily tuned by varying the W_1 dimension of the center edge of the E-shaped slot as shown in Fig. 4(a). It is quite obvious that the variation in W_1 changes only lower resonant frequency, while there is almost no

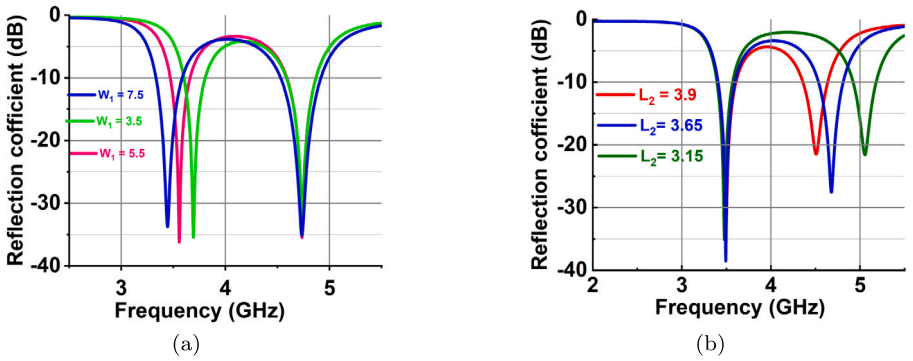

Fig. 4. Parametric analysis to verify independent tuning in each frequency band. (a) variation in W_1, (b) variation in L_2.

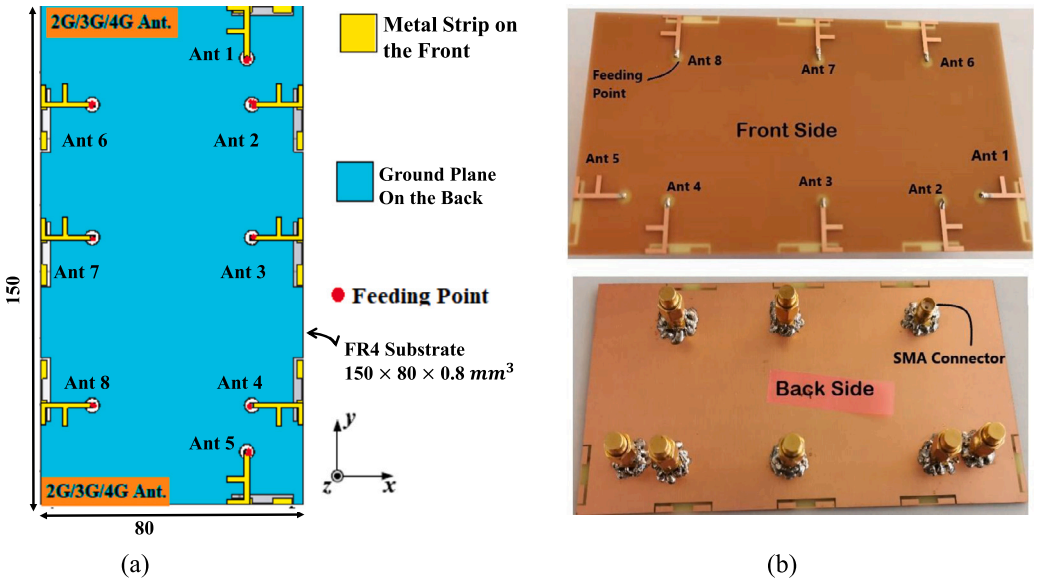

Fig. 5. (a) The 8x8 MIMO proposed antenna configuration, (b) fabricated front and back sides of the MIMO antenna prototype.

effect on the higher resonant frequency. In a similar manner, the L_2 dimension of the upper stub of the F-shaped probe can be used to control the higher resonant frequency, independently, with no impact on the lower resonant frequency as depicted in Fig. 4(b). So, W_1 and L_2 are the two key parameters to tune easily and independently the proposed dual-band antenna element at desired frequencies.

3. MIMO antenna performances

In this section, the simulated and the measured performances of the 8-element MIMO antenna configuration are analyzed with regard to s-parameters, isolation, diversity gain, channel capacity loss, and radiation performance.

3.1. Scattering parameters and isolation

The geometry of the 8-element MIMO antenna is illustrated in Fig. 5(a). The system substrate size is 150 mm × 80 mm × 0.8 mm, which is the same as utilized in a 6-inches size smartphone. All the dual-band antennas (namely, Ant-1 to Ant-8) of the 8 × 8 array are arranged on the four edges of the rectangular substrate. Ant-1 and Ant-5 are arranged horizontally on the opposite short edges, while the vertical long opposite edges have Ant-2 to Ant-4 and Ant-6 to Ant-8, respectively. This meticulous arrangement of antenna elements, two of them with an orthogonal arrangement, helped to achieve polarization diversity due to the orthogonal arrangement of the slot elements on short and long edges.

The proposed dual-band independently tunable MIMO antenna configuration is also simulated using CST Microwave Studio. The prototype of the 8 × 8 MIMO antenna configuration is fabricated and tested to validate antenna performance. The front and back sides of the fabricated 8-element MIMO antenna are depicted in Fig. 5(b). The simulated and experimental s-parameters for

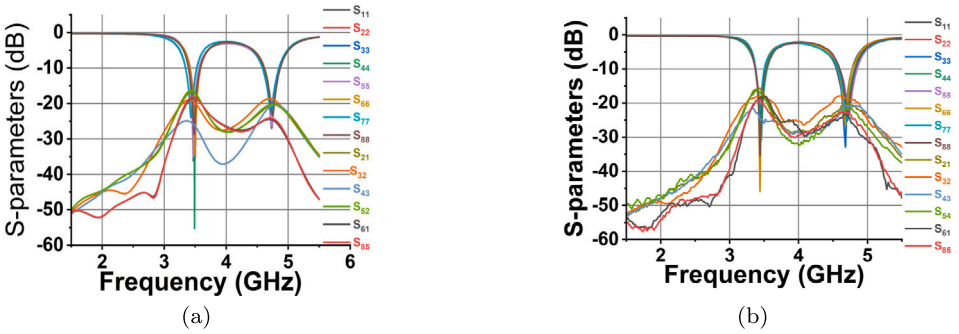

Fig. 6. S-parameters of 8 × 8 MIMO antenna (a) Simulated (b) Measured.

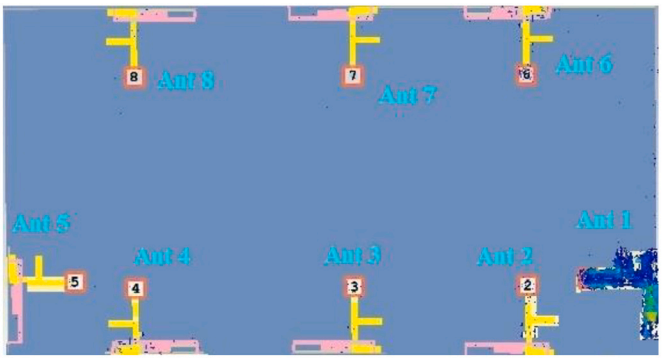

Fig. 7. Surface current distribution on MIMO Antenna due to excitation of Ant-1.

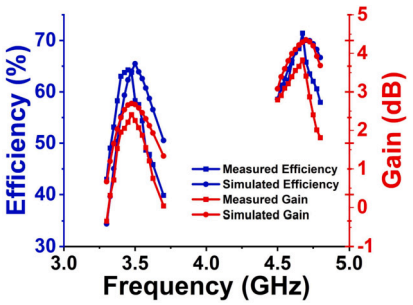

Fig. 8. Efficiency and gain performance for Ant-1.

the proposed dual-band 8-element MIMO antenna are shown in Fig. 6 (a) and (b), respectively. The reflection coefficients and the transmission coefficients for all the 8-elements almost remain the same for both simulated and measured results.

It is evident that both, simulated and measured scattering parameters are in excellent agreement except a minor frequency shift towards the left side is observed in measured results, which may be due to the fabrication tolerance. The simulated and calculated S-parameters exhibit that the proposed dual resonance 8-element MIMO antenna has good impedance bandwidths ($|S_{ii}| > -10$) of 180 MHz at 3.5 GHz and 280 MHz focused at 4.7 GHz frequency bands, respectively, which almost cover the required bandwidths for smartphones operating in the C band at 3.5 GHz and 4.7 GHz frequency bands. The measured transmission coefficients ($|S_{ij}|$), are less than -17 dB in both frequency bands, which depicts good isolation among the elements. The higher isolation among the antenna elements is also verified through surface current distribution analysis. The surface current distribution at 3.5 GHz, when Ant 1 is excited and remaining ports are perfectly matched to 50-ohm impedance, is presented in Fig. 7. A weak coupling effect can be seen due to the excitation of Ant-1 on remaining antenna elements, which confirms the higher isolation between the antenna elements. Similar isolation is observed for the excitation of other antenna elements at both frequencies.

3.2. Radiation performance

Fig. 8, indicates the simulated and measured gain and total efficiencies for Ant-1. The experimental results are again in fine agreement. All antenna efficiencies were measured above 64% across the entire bandwidth. The total measured peak efficiencies for Ant-1 are 64% at 3.5 GHz and 71% at 4.7 GHz, while the measured peak gain is 2.4 dB in the lower frequency band and 3.8 dB

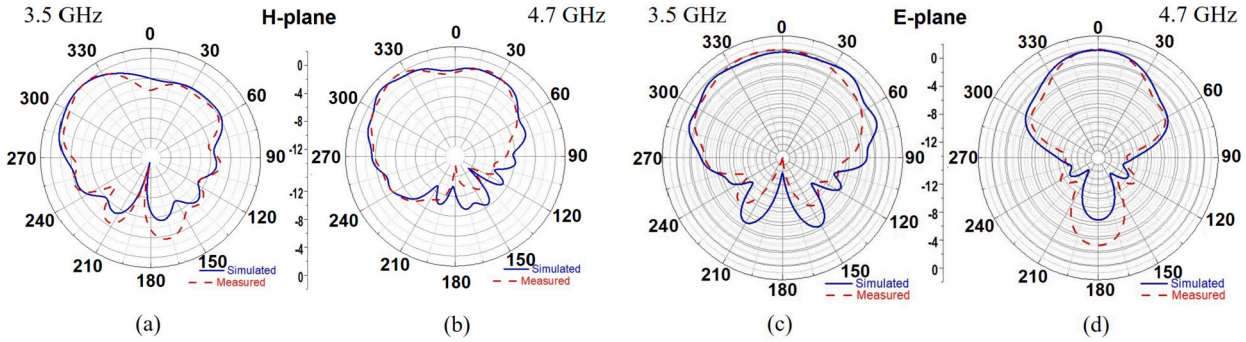

Fig. 9. The normalized radiation patterns of dual-band MIMO antenna (Ant-1) in H-plane at (a) 3.5 GHz, (b) 4.7 GHz, and in E-plane at (c) 3.5 GHz, (d) 4.7 GHz.

Table 2
Performance comparison of multiband 5G MIMO antenna with state-of-the-art.

References	Bandwidth (GHz)	Isolation (dB)	ECC	MIMO Order	Efficiency (%)	Hand Analysis
[4]	4.4 – 5.0	> 18	0.24	8×8	42	Performed
[18]	3.1–3.9	> 12	0.13	8×8	36 – 55	Not Performed
	5.5– 6.3					
[19]	1.6 – 1.9	> 12	0.15	8×8	45	Not Performed
	3.3 - 3.9					
[20]	3.1– 3.85	> 10	0.06	8×8	65–75	Not Performed
	4.8 – 6.0				60–71	
[21]	3.3– 6.6	> 14	0.07	8×8	48–89	Not Performed
[22]	3.4 — 3.93	> 10	0.23	8×8	40–50	Performed
	4.5 - 5.3				60–71	
	3.3 — 6	> 12	0.2	8×8	50–61	Not Performed
Proposed work	3.4 – 3.6	> 17	0.05	8×8	64	Performed
	4.6 — 4.8				71	

in the upper-frequency band. Similar radiation performance is achieved for the remaining antennas, therefor is not shown here for brevity. The simulated and measured H –plane, normalized radiation patterns for the Ant-1 at 3.5 GHz and 4.7 GHz are portrayed in Fig. 9(a) and (b) while the E-plane, normalized radiation patterns for the Ant-1 at 3.5 GHz and 4.7 GHz are presented in Fig. 9(c) and (d) respectively. Where the solid line shows simulation results and the dashed line shows measured results. Both, the simulated and measured radiation patterns are also in decent agreement at both frequencies indicating that the proposed 8-element antenna array has favorable characteristics for 5G mobile phone applications.

3.3. ECC & diversity performances

The signal correlation Envelope Correlation Coefficient (ECC) between the antenna elements is used to measure diversity gain performance for the MIMO antenna. The ECC is computed using s-parameters [17]. Ideally, the ECC should be zero however the minimum acceptable criteria for the 5G MIMO antenna system is (ECC<0.05). The reasonably acceptable performance can be seen for ECC (<0.05), which is close to zero in both the frequency bands [11] and the system also depicts high Diversity Gain (DG) (close to 10 dB), as shown in Fig. 10.

The comprehensive performance comparison of the proposed MIMO antenna with the previously reported multiband MIMO work mainly in terms of antenna type, bandwidth, isolation, ECC, and peak efficiency is presented in Table 2. It is worth mentioning that the proposed dual-band 8-element MIMO antenna has shown isolation (<17 dB) with a slighter cost in terms of peak efficiency (64% & 71%). However, referential work is a poor trade-off between isolation and efficiency as shown in [18,19]. The work presented in [20] is a dual-band 8x8 MIMO design for 5G smartphones with high efficiency (65% -75%) in the lower band and (60% -71%) for higher frequency band, but sacrifices on shallow isolation (<10 dB) that make it unsuitable for the 5G smartphones.

Notably, among all the compared work, only [4,22] have studied hand analysis to investigate the effect of the smartphone user's hand on the performances of multiband 5G MIMO antenna. Similarly, the proposed work has shown superiority in terms of isolation, ECC, and efficiency when compared to [22], which is not only advisable for 5G mobile phone applications due to low isolation (<10 dB), but the use of parasitic sub for miniaturized applications make its design very complex. Therefore, the proposed dual-band 5G MIMO antenna still demonstrates overall exceptional performance so it can be well favorable for 5G smartphones as both the frequency bands are independently tunable with a very simple and compact design structure.

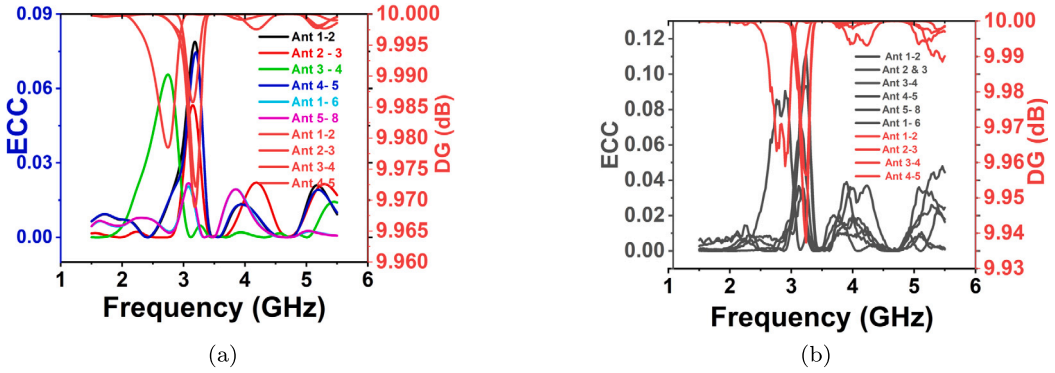

Fig. 10. ECC and DG of the proposed dual-band MIMO antenna. (a) Simulated. (b) Measured.

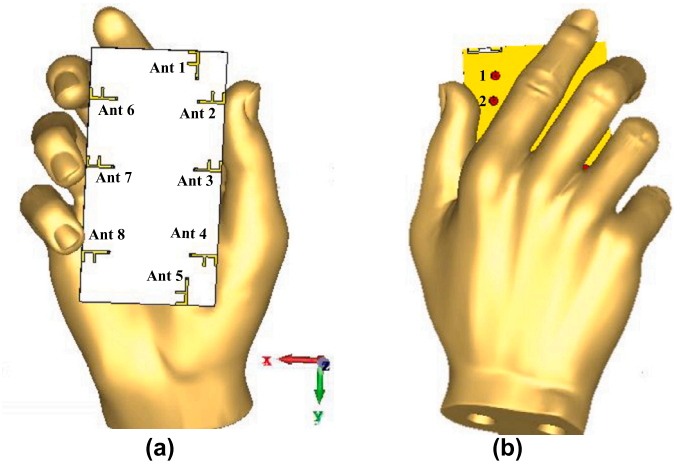

Fig. 11. Hand Analysis (a) Front view, (b) Back.

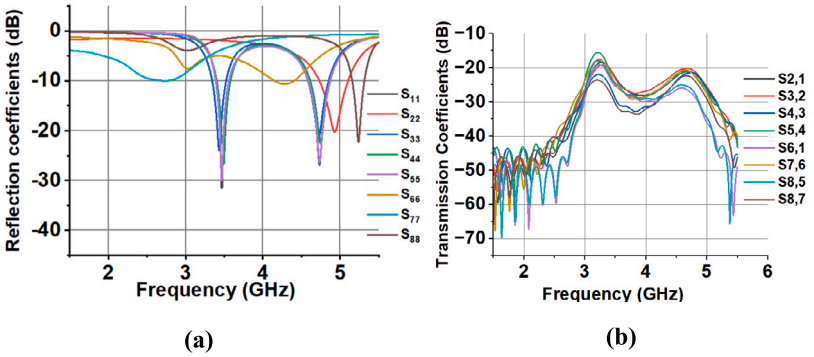

Fig. 12. Simulated (a) reflection coefficients, and (b) transmission coefficients of SHM.

4. Hand analysis

To verify the effect of the mobile phone user's hand on the performance of this proposed multi-band 5G MIMO antenna, the front and back views of the hand phantom are presented in this section as shown in Fig. 11 (a) and (b), respectively. The human hand phantom was imported in CST Microwave Studio version 19, due to which a minor variation in the resonant mode has been observed. The analyses were performed in single-hand mode (SHM) only. The reflection coefficients are depicted in Fig. 12 (a). As Ant. 2, 6, 7, and 8 are in direct contact with the fingers and thumb, not only they are highly affected but also undesirable results can be observed. In addition, Ant. 2, 6, 7, and 8 have illustrated poor impedance matching. Notably, high isolation over 16 dB can still be observed across the operational bandwidth as illustrated in Fig. 12 (b).

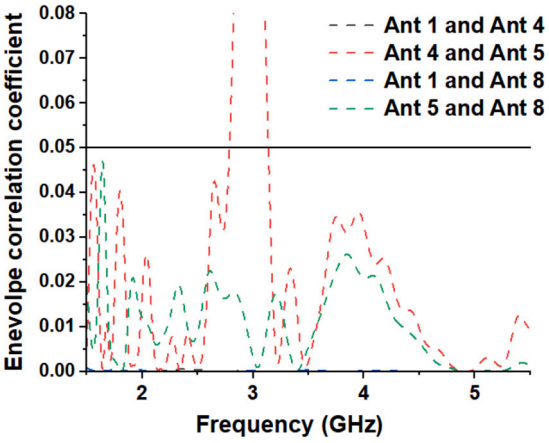

Fig. 13. Simulated ECC for SHM.

Fig. 13 depicts the simulated envelope correlation coefficient of the SHM. The less than 0.05 ECC results demonstrate the desirable diversity performance. Therefore, based on the results of S-parameters and ECC, it can be concluded that the proposed antenna not only has resistance in hand-grip conditions but also has excellent robustness.

5. Conclusion

A novel combination of an E-shaped slot and an F-shaped probe to make this design dual-band-independently tunable 8-element MIMO antenna effectively working for 5G mobile-phone working in sub-6 GHz (3.5 GHz and 4.7 GHz) frequency bands is presented in this paper. The proposed dual-band E-shaped slot antenna element is designed without using any external decoupling structure making this design extremely simple, compact, and easy to integrate with narrow-frame 4G/5G smartphones. The enhanced isolation (>17 dB) with suitable peak efficiency (64% & 71%), and low ECC (< 0.05) are significant features of the proposed 8-element MIMO antenna. The measured results also exhibit a decent agreement with simulated results in both frequency bands, which confirms that it is suitable for working in the sub-6 GHz band to attain the required spectral efficiency. Consequently, the proposed independently tunable dual-band MIMO antenna is a simple but effective design with great inherent isolation, high diversity performance and efficiency, and straightforward implementation, making it a promising candidate for 5G smartphone applications operating in sub-6 GHz frequency bands not only in the current but also in future mobile devices. The antenna size reduction, exploring the millimeter wave (mmWave) band, and transforming this proposed 8-element antenna into massive MIMO (mMIMO) by increasing the number of antennas is the future aspect.

CRediT authorship contribution statement

Ali Sufyan: Conceptualization, Methodology, Software, Writing – original draft. **Khan Bahadar Khan:** Data curation, Project administration, Supervision. **Xingliang Zhang:** Investigation, Resources, Visualization. **Tauseef Ahmad Siddiqui:** Formal analysis, Writing – review & editing. **Abdul Aziz:** Supervision, Validation, Visualization.

Declaration of competing interest

The authors declare that they have no known competing financial interests or personal relationships that could have appeared to influence the work reported in this paper.

References

[1] Y. Li, Z. Zhao, Z. Tang, Y. Yin, A low-profile, dual-band filtering antenna with high selectivity for 5g sub-6 GHz applications, Microw. Opt. Technol. Lett. 61 (10) (2019) 2282–2287.
[2] Y. Li, Y. Luo, G. Yang, et al., High-isolation 3.5 GHz eight-antenna mimo array using balanced open-slot antenna element for 5g smartphones, IEEE Trans. Antennas Propag. 67 (6) (2019) 3820–3830.
[3] L. Chang, Y. Yu, K. Wei, H. Wang, Orthogonally polarized dual antenna pair with high isolation and balanced high performance for 5g mimo smartphone, IEEE Trans. Antennas Propag. 68 (5) (2020) 3487–3495.
[4] B. Cheng, Z. Du, A wideband low-profile microstrip mimo antenna for 5g mobile phones, IEEE Trans. Antennas Propag. 70 (2) (2021) 1476–1481.
[5] H. Babashah, H.R. Hassani, S. Mohammad-Ali-Nezhad, A compact uwb printed monopole mimo antenna with mutual coupling reduction, Prog. Electromagn. Res. C 91 (2019) 55–67.
[6] L. Sun, Y. Li, Z. Zhang, M.F. Iskander, A compact planar omnidirectional mimo array antenna with pattern phase diversity using folded dipole element, IEEE Trans. Antennas Propag. 67 (3) (2018) 1688–1696.
[7] J. Zhu, S. Li, S. Liao, Q. Xue, Wideband low-profile highly isolated mimo antenna with artificial magnetic conductor, IEEE Antennas Wirel. Propag. Lett. 17 (3) (2018) 458–462.

[8] N. Jaglan, S.D. Gupta, B.K. Kanaujia, M.S. Sharawi, 10 element sub-6-GHz multi-band double-t based mimo antenna system for 5g smartphones, IEEE Access 9 (2021) 118662–118672.
[9] T. Pei, L. Zhu, J. Wang, W. Wu, A low-profile decoupling structure for mutual coupling suppression in mimo patch antenna, IEEE Trans. Antennas Propag. 69 (10) (2021) 6145–6153.
[10] L. Sun, Y. Li, Z. Zhang, Wideband decoupling of integrated slot antenna pairs for 5g smartphones, IEEE Trans. Antennas Propag. 69 (4) (2020) 2386–2391.
[11] Y.Q. Hei, J.G. He, W.T. Li, Wideband decoupled 8-element mimo antenna for 5g mobile terminal applications, IEEE Antennas Wirel. Propag. Lett. 20 (8) (2021) 1448–1452.
[12] W. Hu, X. Liu, S. Gao, L.-H. Wen, L. Qian, T. Feng, R. Xu, P. Fei, Y. Liu, Dual-band ten-element mimo array based on dual-mode ifas for 5g terminal applications, IEEE Access 7 (2019) 178476–178485.
[13] N. Behdad, K. Sarabandi, Dual-band reconfigurable antenna with a very wide tunability range, IEEE Trans. Antennas Propag. 54 (2) (2006) 409–416.
[14] A. Zaidi, W.A. Awan, N. Hussain, A. Baghdad, A wide and tri-band flexible antennas with independently controllable notch bands for sub-6-GHz communication system, Radioengineering 29 (1) (2020).
[15] N.-W. Liu, L. Zhu, W.-W. Choi, X. Zhang, A low-profile aperture-coupled microstrip antenna with enhanced bandwidth under dual resonance, IEEE Trans. Antennas Propag. 65 (3) (2017) 1055–1062.
[16] B. Kibret, A.K. Teshome, D.T. Lai, Characterizing the human body as a monopole antenna, IEEE Trans. Antennas Propag. 63 (10) (2015) 4384–4392.
[17] R. Chandel, A.K. Gautam, K. Rambabu, Design and packaging of an eye-shaped multiple-input–multiple-output antenna with high isolation for wireless uwb applications, IEEE Trans. Compon. Packag. Manuf. Technol. 8 (4) (2018) 635–642.
[18] M.N. Zahid, Z. Gaofeng, S.H. Kiani, U. Rafique, S.M. Abbas, M. Alibakhshikenari, M. Dalarsson, H-shaped eight-element dual-band mimo antenna for sub-6 GHz 5g smartphone applications, IEEE Access 10 (2022) 85619–85629.
[19] R.K. Mistri, S.K. Mahto, R. Sinha, Dual band 8×8 mimo antenna system for dcs 1800 and 5g mobile applications, Int. J. Commun. Syst. 36 (3) (2023) e5387.
[20] D. Serghiou, M. Khalily, V. Singh, A. Araghi, R. Tafazolli, Sub-6 GHz dual-band 8× 8 mimo antenna for 5g smartphones, IEEE Antennas Wirel. Propag. Lett. 19 (9) (2020) 1546–1550.
[21] N. Sghaier, L. Latrach, A. Gharsallah, Design of a dual-polarized uwb 5g nr antenna, Wirel. Pers. Commun. (2022) 1–18.
[22] Z. Chen, Y. Liu, T. Yuan, H. Wong, A miniaturized mimo antenna with dual-band for 5g smartphone application, IEEE Open J. Antennas Propag. (2023).